Energy density functional approaches to inhomogeneous superfluid neutron-star matter

Nakatsukasa, Takashi

University of Tsukuba

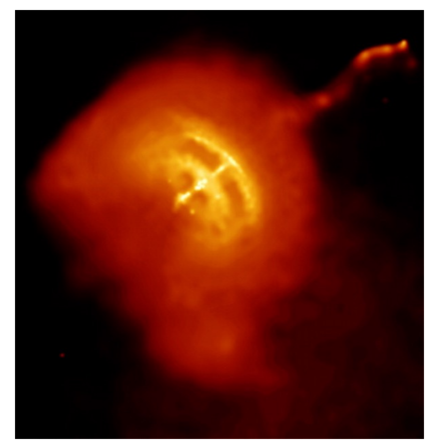

Supported by

TOMOE

ERATO

科研費 KAKENHI

QNP2024 @Barcelona, Spain, 2024.7.8-12

Contents

- Fermi Operator Expansion (FOE) method
- Self-consistent description of the inner crust
  - Band calculation for 1D slab (lasagna) phase
  - Effect of superfluidity
- Finite-temperature HFB in the 3D coordinate-space representation
  - Toward 2D, 3D phases

Crust of neutron stars

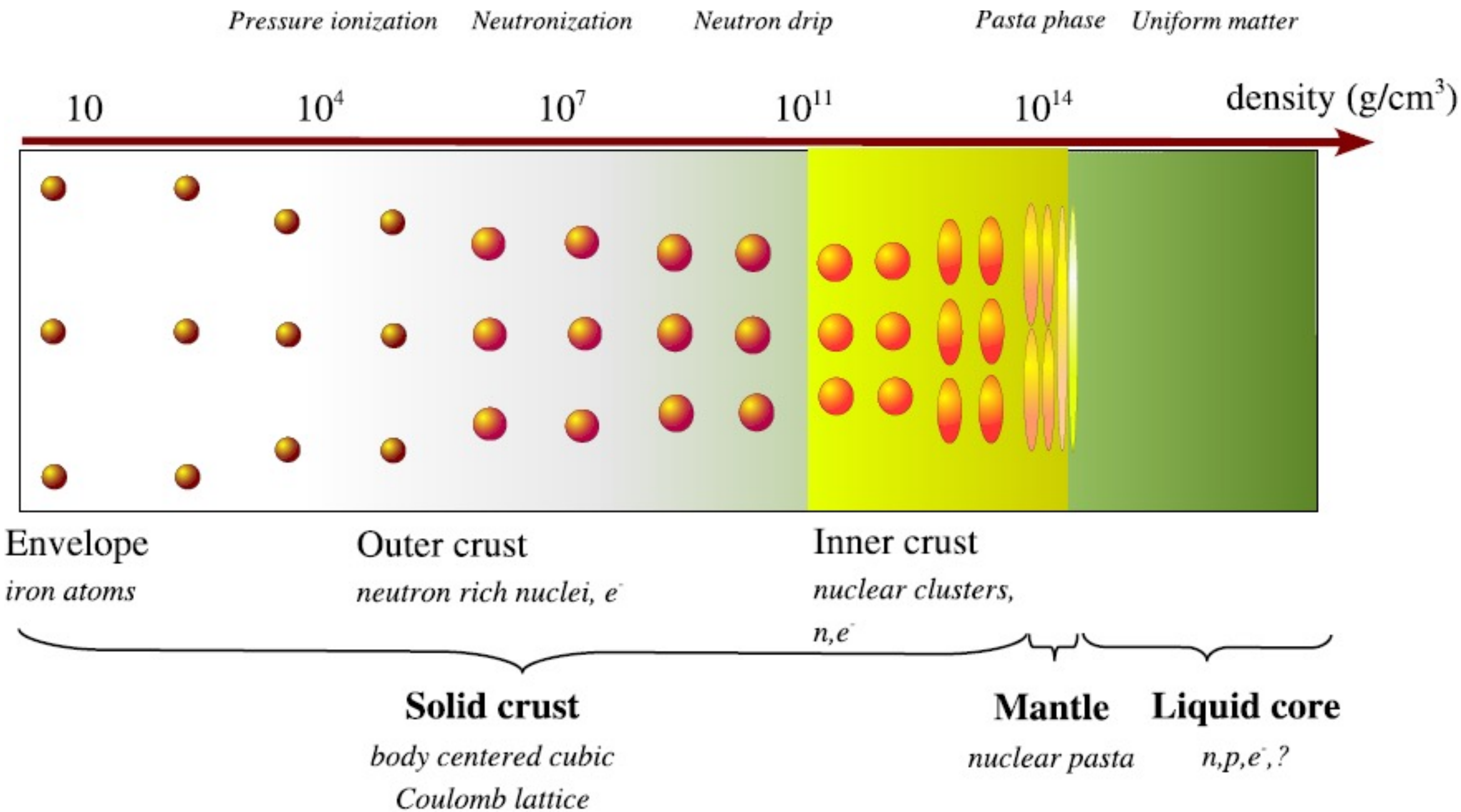

Chamel and Haensel, Living Rev. Relativity **11**, 10 (2008)

Inner crust

($\rho_0 = 3 \times 10^{14}$ g cm^{-3})

$0.001\rho_0$

$0.5\ \rho_0$

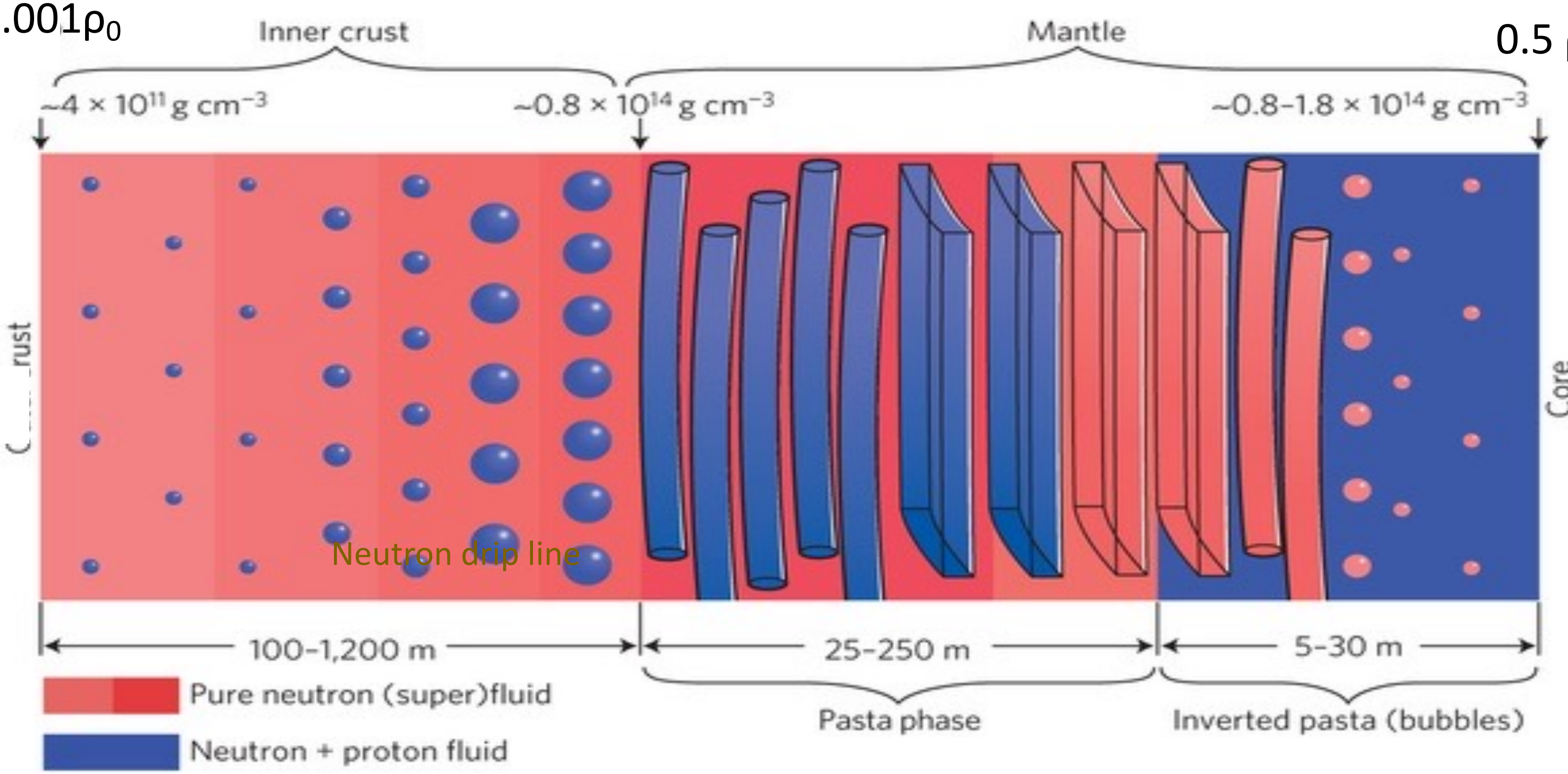

William G. Newton (2013)

Nuclei beyond the neutron drip line

+ low-density neutrons gas

+ electrons gas

Phenomena associated with crust

- Crustal oscillation

Low frequency oscillation

Sotani et al.: Phys. Rev. Lett **108** (2012) 201101.

- Cooling process

Direct URCA process

Gusakov et al.: A&A **421** (2004) 1143.

Low thermal conductivity

Horowitz et al.: Phys. Rev. Lett. **114** (2015) 031102.

- Pulsar glitch

Entrainment for conduction neutrons

B. Carter et al.: Int. J. Mod. Phys. D **15**(2006) 777.

Static crust structure

Dynamic transport properties

Energy density functional method

- Energy density functional $E[\rho, \kappa]$
  - ρ: One-body density
  - κ: Pair density (abnormal density)

- Potentials
  - $V = \delta E / \delta \rho$: One-body (Kohn-Sham) potential
  - $\Delta = \delta E / \delta \kappa^*$: One-body (Kohn-Sham

- Kohn-Sham-Bogoliubov equation
  - $$\begin{pmatrix} h - \mu & \Delta \\ -\Delta^* & -(h - \mu)^* \end{pmatrix} \begin{pmatrix} U_k \\ V_k \end{pmatrix} = E_k \begin{pmatrix} U_k \\ V_k \end{pmatrix}$$
  - Diagonalization produces $\rho = V^* V^T, \kappa = V^* U^T$
- Diagonalization requires cost of computation $\propto N^3$

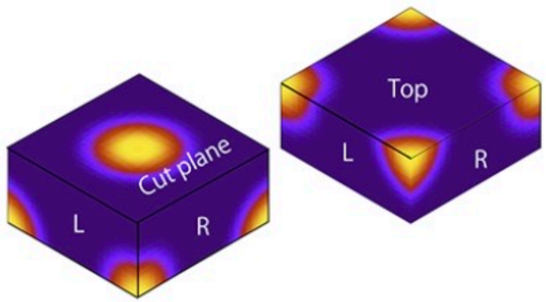

EDITORS' SUGGESTION

Fermi operator expansion method for nuclei and inhomogeneous matter with a nuclear energy density functional

Calculations for nuclear structure at high excitation energy or of nuclear matter in explosive stellar phenomena and neutron stars require intensive computations. The author tests the performance of a numerical method based on Fermi operator expansion that requires neither diagonalization nor Gram-Schmidt orthonormalization. The approach is suitable for massively parallel computing with distributed memory, and the calculations promise to scale well for large space sizes. Applied to finite nuclei and inhomogeneous nuclear matter, the method is efficient at high temperature, and the calculations clearly show the liquid-gas phase transition.

Takashi Nakatsukasa

Phys. Rev. C **107**, 015802 (2023)

Density operator at finite T

- Fermi-Dirac distribution function

$$f_T(E) = \left(1 + e^{\beta(E-\mu)}\right)^{-1}$$

- Fermi-Dirac distribution operator

$$f_T(\hat{H}) = \left(1 + e^{\beta(\hat{H}-\mu)}\right)^{-1}$$

- One-body density

$$H|n\rangle = E_n|n\rangle$$

$$\rho_T = \sum_n |n\rangle f_T(E_n)\langle n| = f_T\left(\hat{H}\right) \approx \sum_{k=0}^{M} a_k T_k(\hat{H})$$

Chebyshev expansion of $f_T(E)$

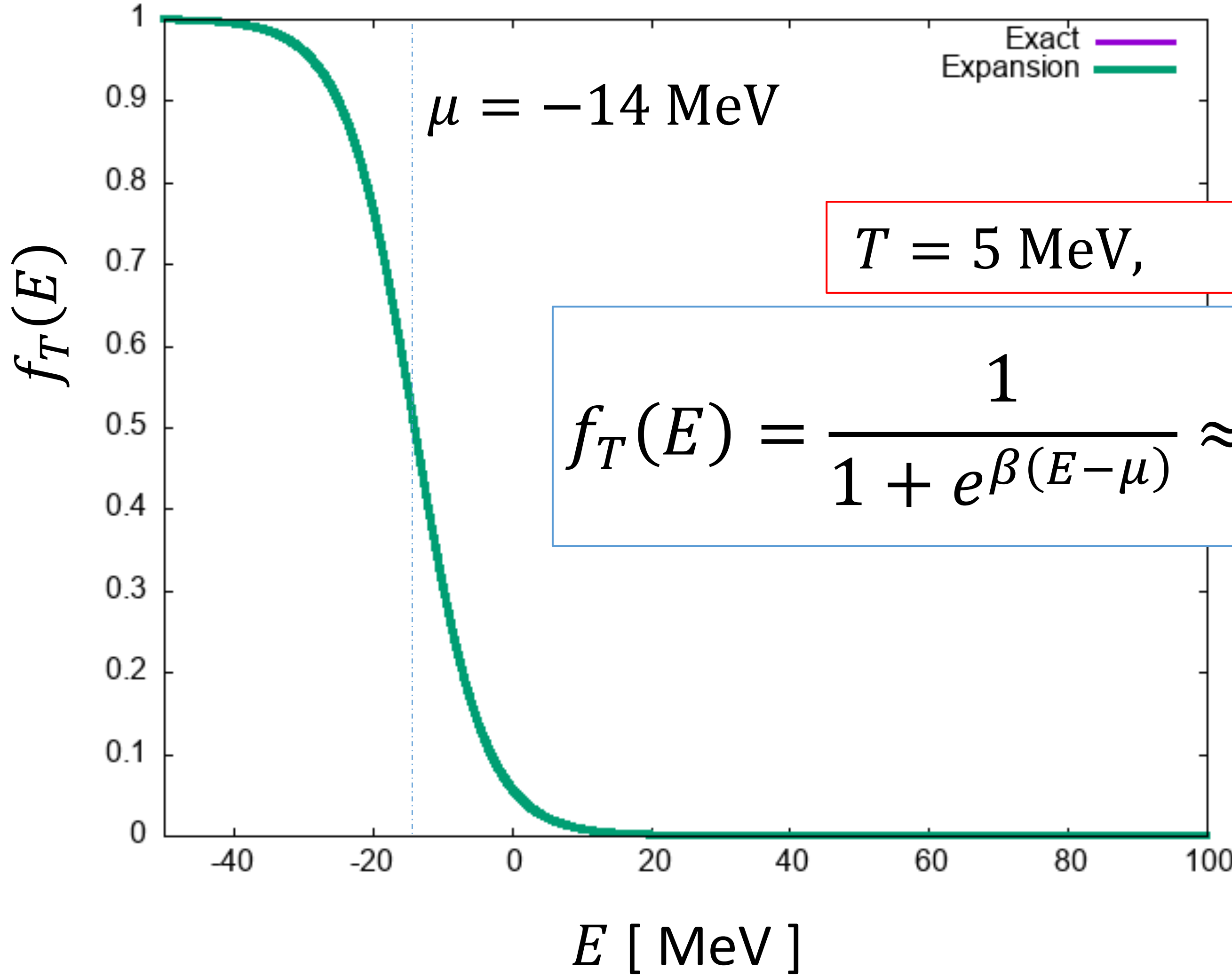

$T = 5$ MeV, $\quad M = 200$

$$f_T(E) = \frac{1}{1 + e^{\beta(E-\mu)}} \approx \sum_{k=0}^{M} a_k T_k(E)$$

Code

- Test Fortran code with MPI+OpenMP
- Energy density functional *w/o pairing*
  - Rectangular box with periodic boundary condition
  - FFT to construct the Coulomb potential
  - Kinetic energy computed with the finite difference
  - 3D square lattice

$$\rho_T |\vec{r}\rangle = \sum_{k=0}^{M} a_k T_k(H) |\vec{r}\rangle$$

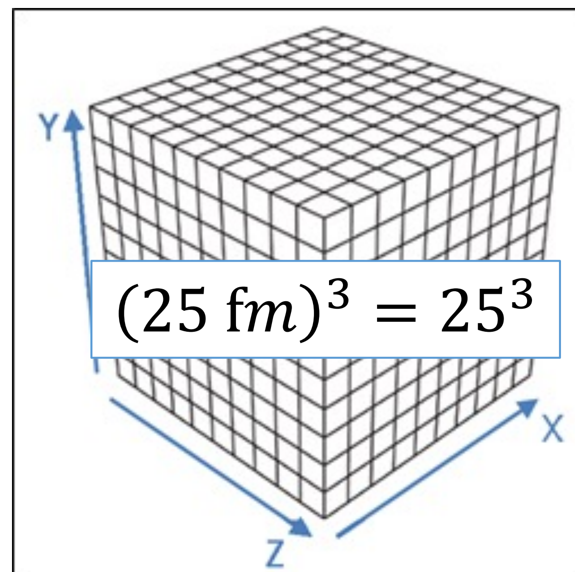

Shape phase transition: ^{24}Mg

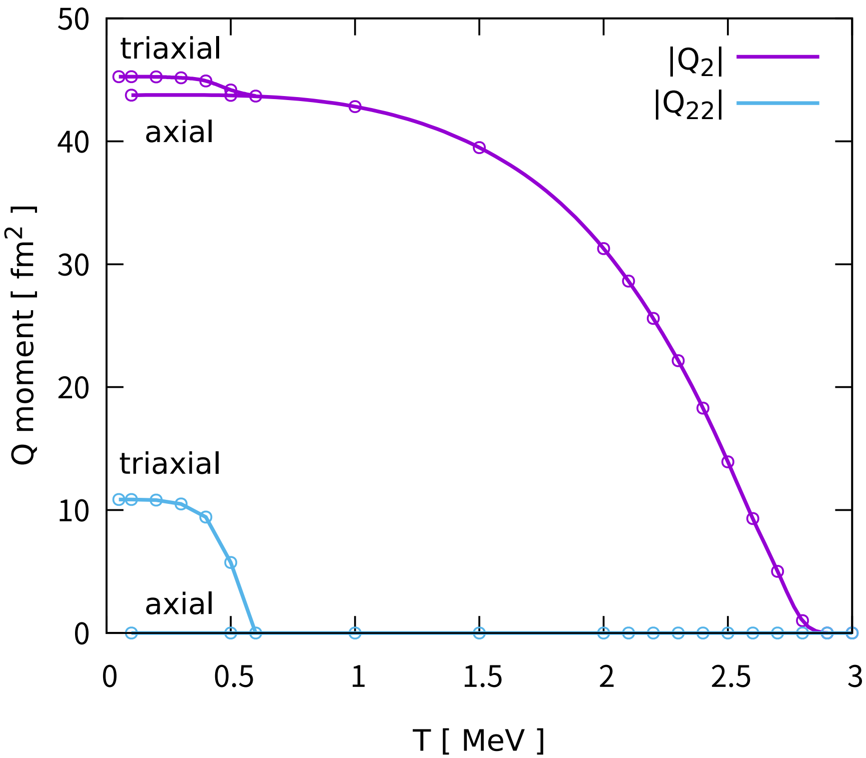

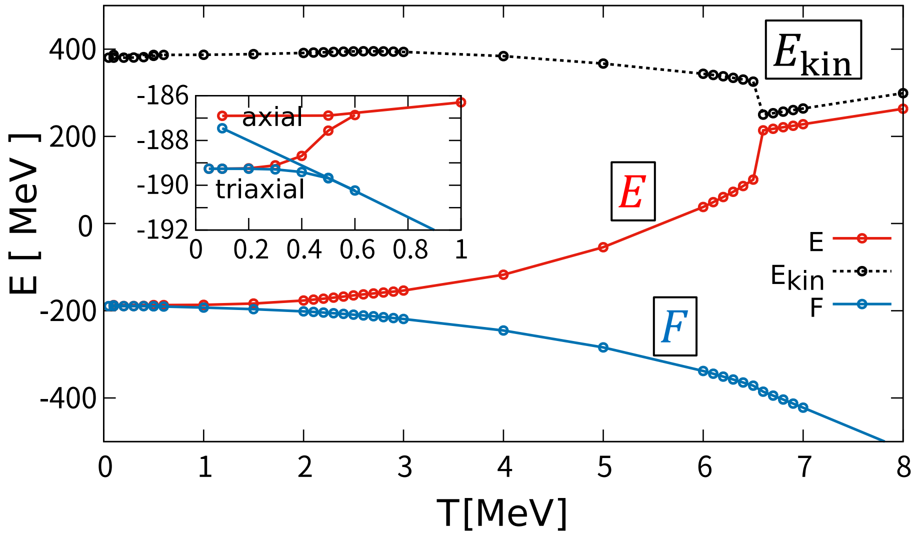

Inhomogeneous symmetric nuclear matter

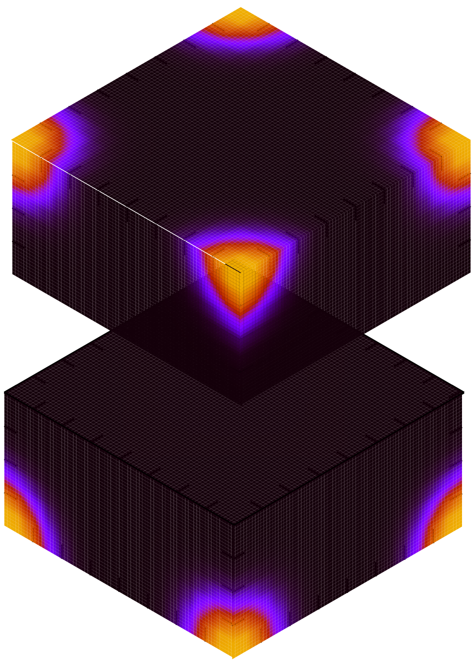

$T = 5$ MeV

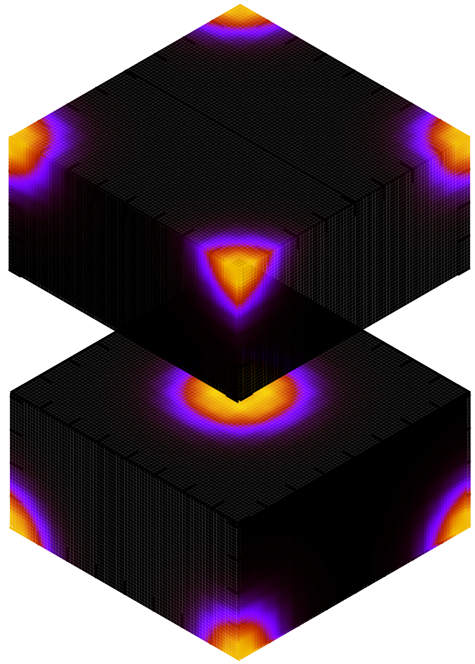

$T = 2$ MeV

Box: $(23\ \mathrm{fm})^3$
$n_b = 2.63 \times 10^{-3}\ \mathrm{fm}^{-3}$

From Bcc to simple cubic

Order-N

- Iterative computation of $T_k(H)|i\rangle$

$$H|\vec{r}\rangle = \sum_{\vec{d}} c_{\vec{d}} |\vec{r} + \vec{d}\rangle$$

- Calculation of $\rho_T(\vec{r}, \vec{r}\,')$ requires only a region around $\vec{r}\,'$
- Truncation for $H^n|\vec{r}\rangle$, setting $c_{\vec{d}} = 0$ for $|\vec{d}| > d_0$

$$H^n|\vec{r}\rangle = \sum_{\vec{d}} c_{\vec{d}} |\vec{r} + \vec{d}\rangle$$

$\Rightarrow$ $\boxed{\text{Order-}N}$

Wu, Jayanthi, Phys. Rep. 358 (2002) 1

Off-diagonal elements of $\rho(0, \vec{r})$

$\rho_B = 0.03\ \mathrm{fm}^{-3}$

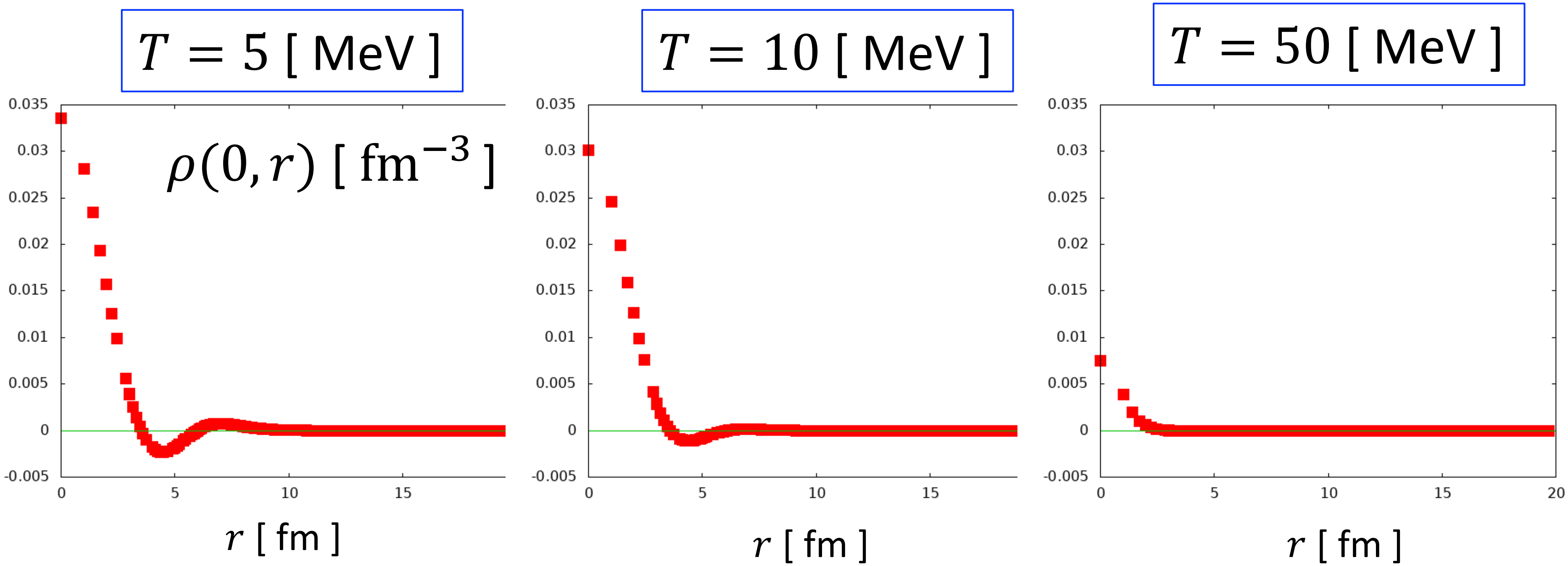

Off-diagonal elements of $\rho(0, \vec{r})$

$\rho_B = 0.03 \text{ fm}^{-3}$

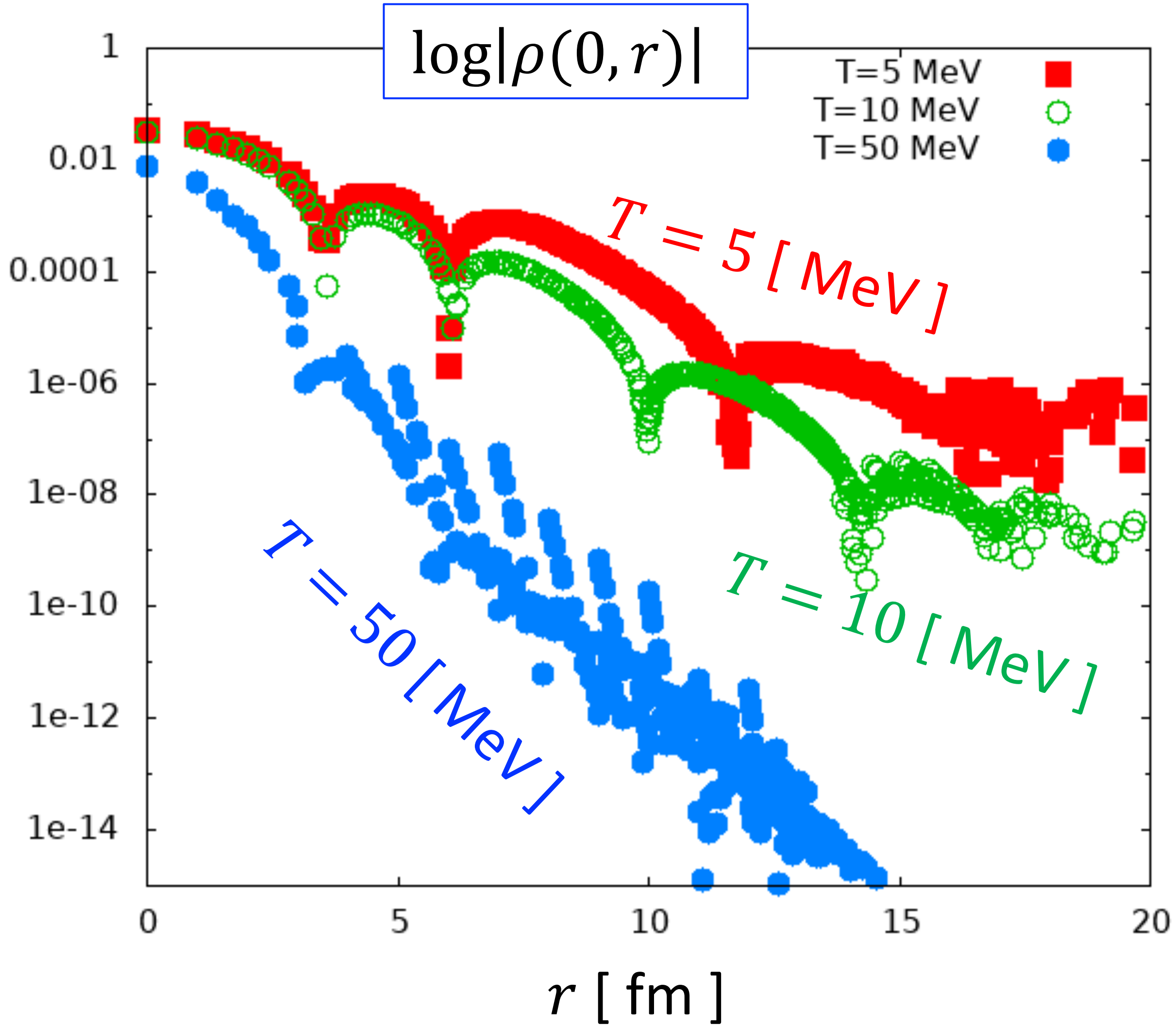

Pulsar glitch

Most promising glitch mechanisms

- Vortex pinning-unpinning (Anderson-Itoh 1975; Alper et al. 1981, 1993, 1996)
- Glitch origin: Inner crust

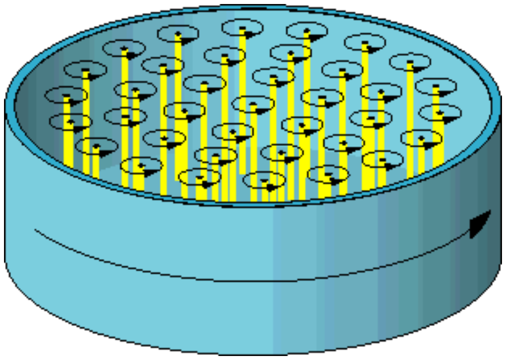

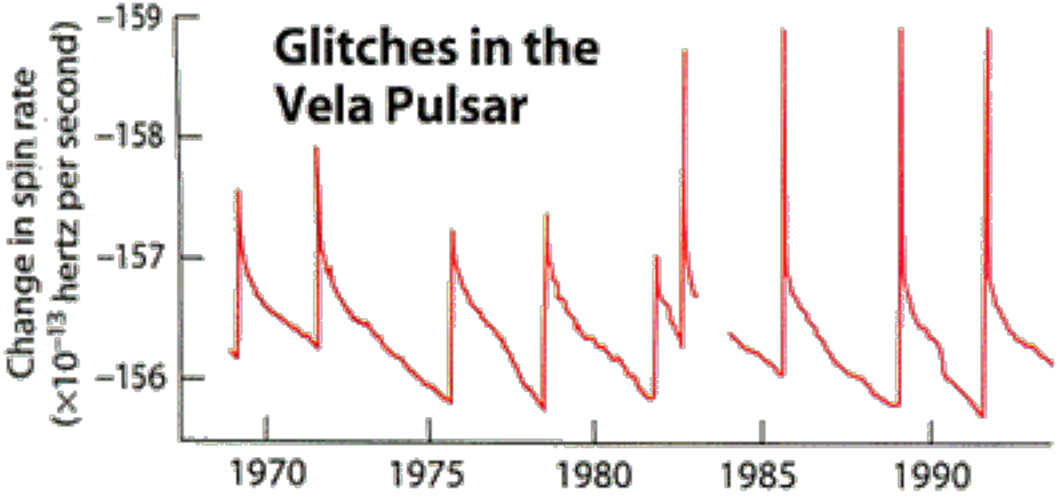

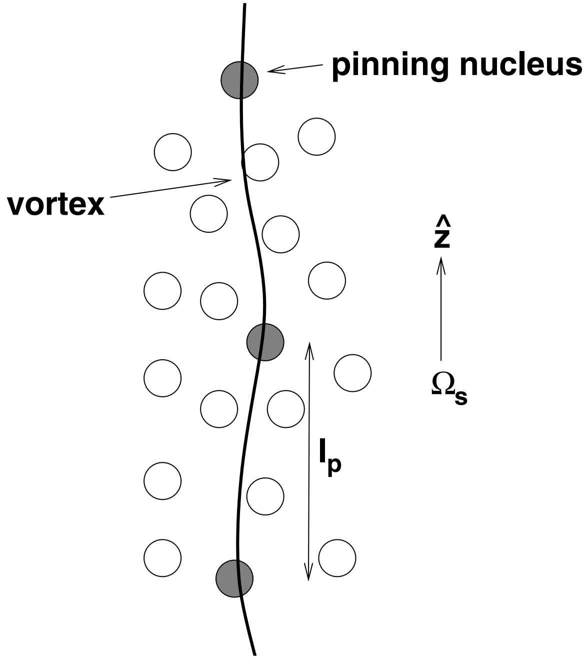

Observation constraint

Andersson et al., PRL 109, 241103 (2012)

Moment of inertia ratio (I_n: Neutron MoI, I: Total MoI)

$$\boxed{I_n/I \approx 2\tau_c \mathcal{A}, \quad \text{where } \mathcal{A} = \frac{1}{t_{\rm obs}}\left(\sum_i \Delta\Omega_p^i/\Omega_p\right).}$$

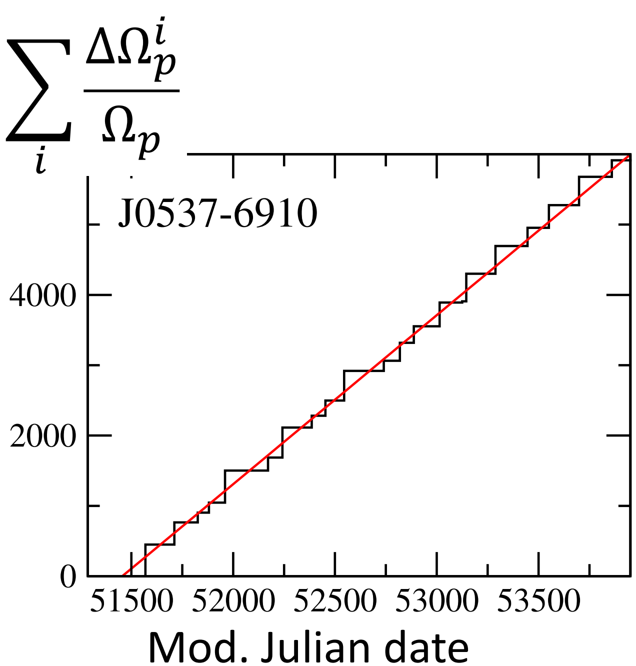

Characteristic age of pulsar $\tau_c = -\frac{\Omega_p}{2\dot{\Omega}_p}$

PSR	τ_c (kyr)	$\mathcal{A}$ $(\times 10^{-9}/d)$	I_n/I (%)
J0537-6910	4.93	2.40	0.9
B0833-45 (Vela)	11.3	1.91	1.6
J0631+1036	43.6	0.48	1.5
B1338-62	12.1	1.31	1.2
B1737-30	20.6	0.79	1.2
B1757-24	15.5	1.35	1.5
B1758-23	58.4	0.24	1.0
B1800-21	15.8	1.57	1.8
B1823-13	21.5	0.78	1.2
B1930+22	38.8	0.95	2.7
J2229+6114	10.5	0.63	0.5

Observation constraint

Andersson et al., PRL 109, 241103 (2012)

Moment of inertia ratio (I_n: Neutron MoI, I: Total MoI)

$$I_n/I \approx 2\tau_c \mathcal{A}, \quad \text{where } \mathcal{A} = \frac{1}{t_{\mathrm{obs}}}\left(\sum_i \Delta\Omega_p^i/\Omega_p\right).$$

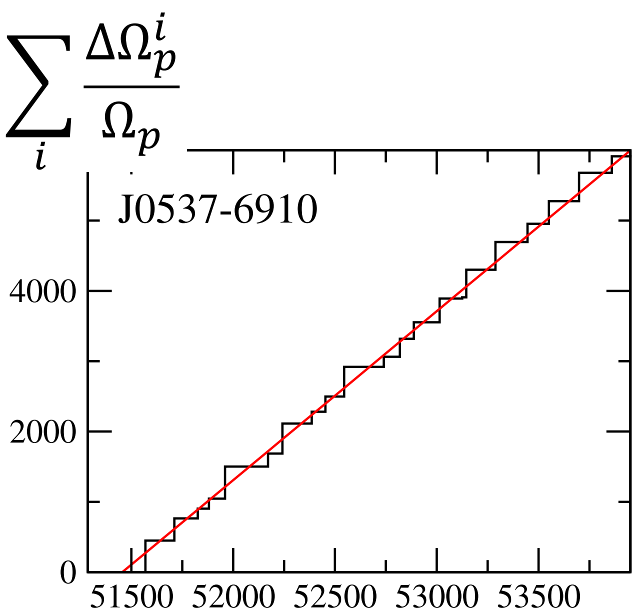

Mod. Julian date

Characteristic age of pulsar $\tau_c = -\frac{\Omega_p}{2\dot{\Omega}_p}$

PSR	τ_c (kyr)	$\mathcal{A}$ ($\times 10^{-9}/d$)	I_n/I (%)
J0537-6910	4.93	2.40	0.9
B0833-45 (Vela)	11.3	1.91	1.6
J0631+1036	43.6	0.48	1.5
B1338-62	12.1	1.31	1.2
B1737-30	20.6	0.79	1.2
B1757-24	15.5	1.35	1.5
B1758-23	58.4	0.24	1.0
B1800-21	15.8	1.57	1.8
B1823-13	21.5	0.78	1.2
B1[illegible]	[illegible]	[illegible]	2.7
J22[illegible]	[illegible]	[illegible]	0.5

These ratios are consistent with the superfluid neutrons in the inner crust.

Entrainment effect

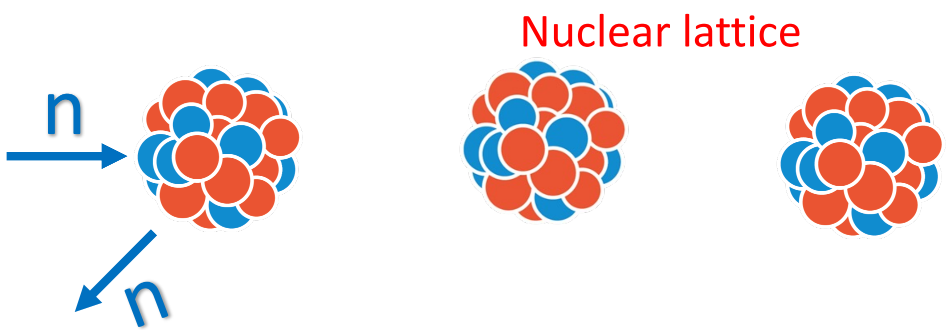

N. Chamel, PRC 85, 035801 (2012)

Neutron gas is not "free".
Neutron mobility is significantly reduced.

Bragg scattering

$$\frac{m_n^*}{m_n} \gtrsim 10$$

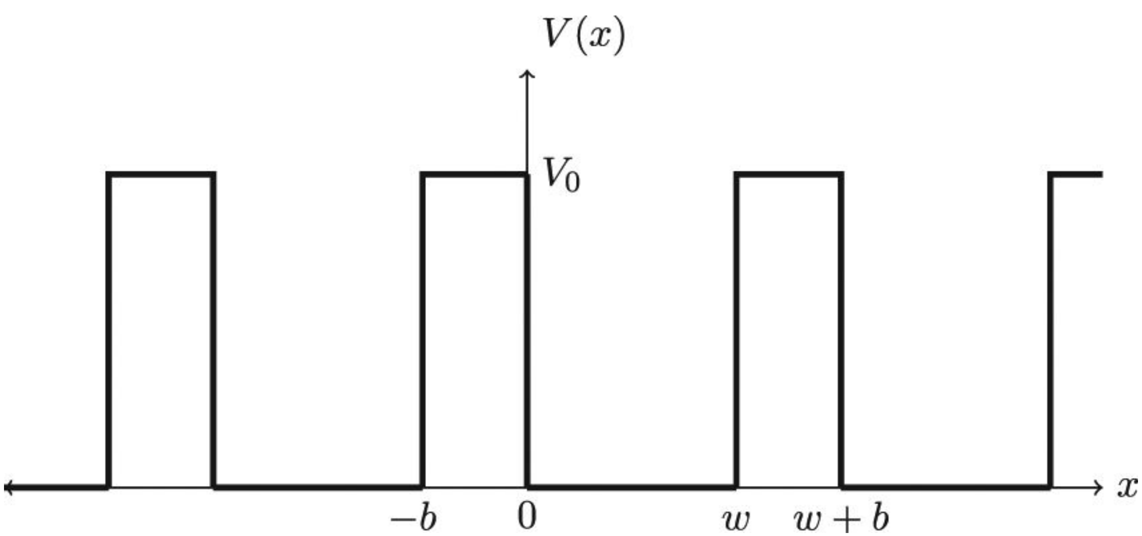

Observation constraint (mod.)

Andersson et al., PRL 109, 241103 (2012)

Moments of inertia ratio with entrainment

$$\frac{I_n}{I} \approx 2\tau_c \mathcal{A} \frac{\langle m_n^* \rangle}{m_n} \text{ where } \mathcal{A} = \frac{1}{t_{\mathrm{obs}}}\left(\sum_i \Delta\Omega_p^i / \Omega_p\right).$$

Need more superfluid neutrons in the crust

Contradiction with standard nuclear matter EOS

Effective masses

- (Microscopic) effective mass due to velocity-dependent potential

$$\frac{m^*}{m} \sim 0.7 - 0.8 \quad \rightarrow \quad \frac{m^*}{m} = 1$$

- (Macroscopic) effective mass due to Bragg scattering of periodic potential

$\frac{m^*}{m}$ can be very large/small or even negative

Energy functional

Barcelona-Catania-Paris-Madrid(BCPM) density functional

M. Baldo, L. M. Robledo, X. Vinas, Phys.Rev.C87,064305(2013)

- Volume term : local density approximations

based on ab initio nuclear and neutron matter EOS

(m*/m = 1, L=52.96 MeV, K_0=212.4 MeV)

$$E_{vol} = \int dr \left[\left(1 - \beta^2(r)\right) \sum_{n=1}^{5} a_n \rho^n(r) + \beta^2(r) \sum_{n=1}^{5} b_n \rho^n(r) \right] \rho(r)$$

- Surface term : Gaussian folding

fixing binding energy of finite 579 even-even nuclei

$$E_{suf} = \sum_{q,q'=p,n} V_{qq'} \left[\int drdr' \rho_q(r) \rho_{q'}(r') e^{-(r-r')^2/r_0{}^\wedge 2} - \int dr e^{-r^2/r_0^2} \int dr' \rho_q(r') \rho_{q'}(r') \right]$$

Band calculation of inner crust

- Treatment of dripped neutrons
- Self-consistent band calculation
  - Large space = Many Bloch ***k***
  - Structure optimization “without external potentials”

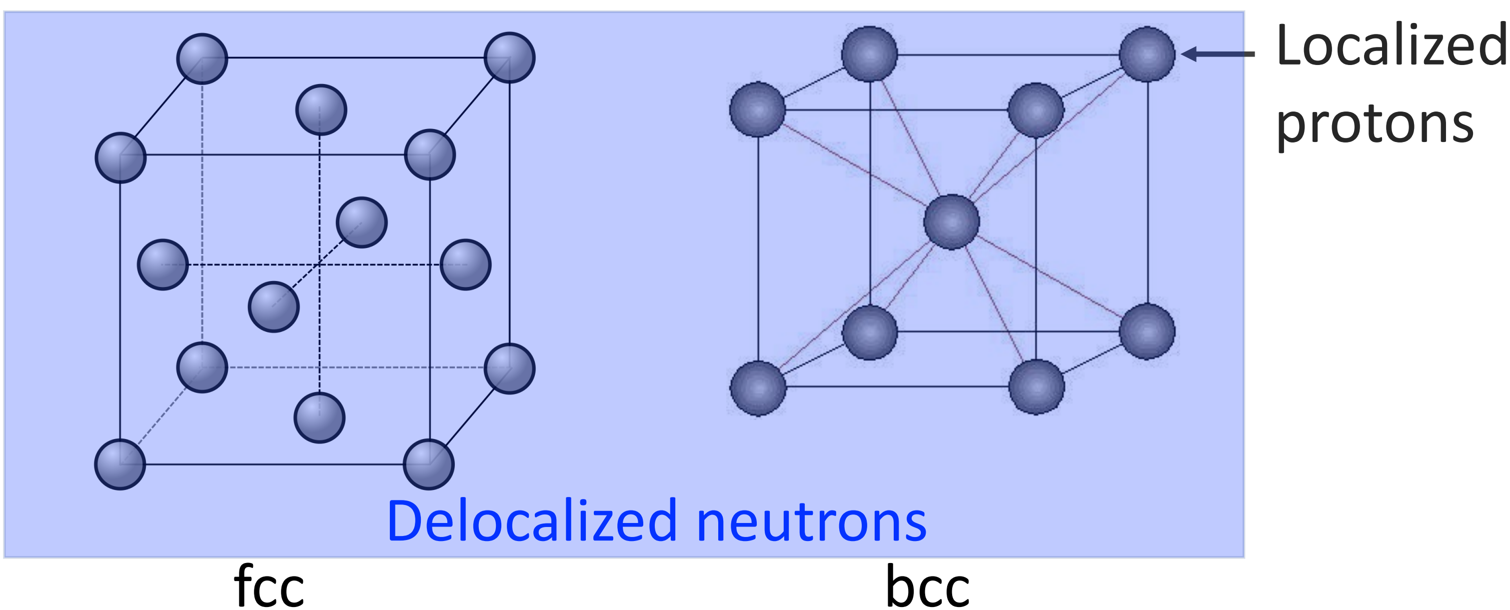

Band calculation

- Single-particle states in a periodic potential
  - Bulk matter → Unit cell with many Bloch wave numbers $\boldsymbol{k}$
- Effect of Bragg scattering (entrainment)
  - $\boldsymbol{k}$-dependence of bands

- Former calculations (Chamel et al.)
  - Thomas-Fermi appox. to fix the potential
- Present work: Self-consistent band cal.
  - 1D slab phase, near the crust bottom

Gnocchi (droplet)

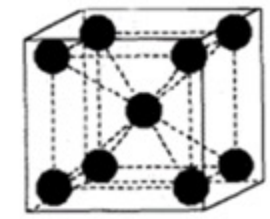

(a)

Spaghetti (rod)

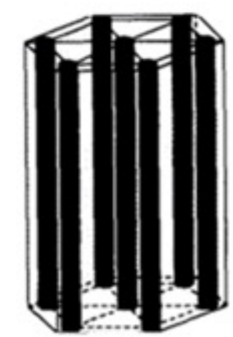

(b)

Lasagna (slab)

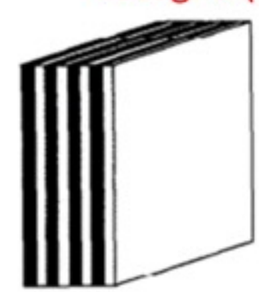

(c)

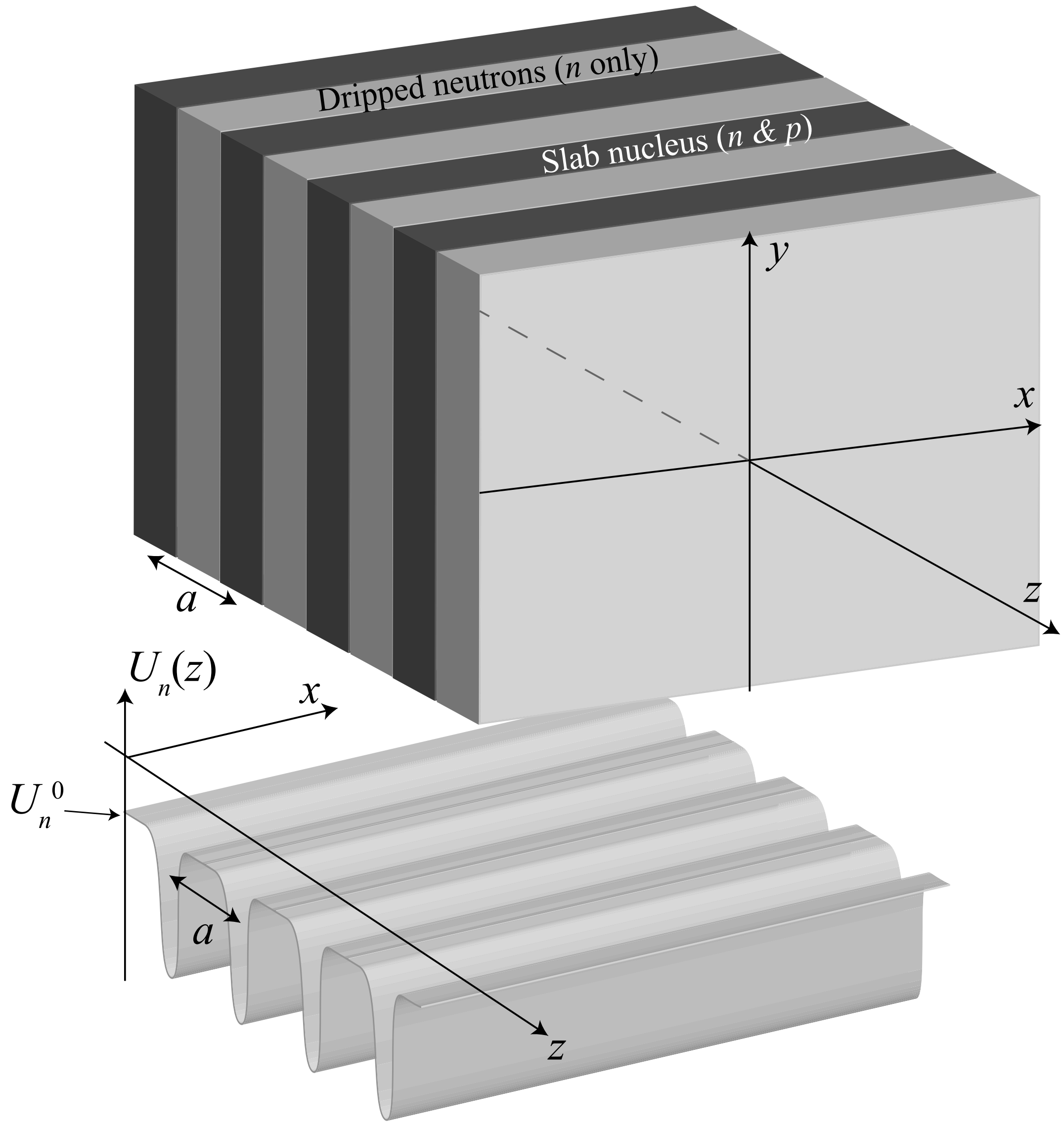

Dripped neutrons (n only)
Slab nucleus (n & p)
y
x
z
a
$U_n(z)$
x
$U_n^{\ 0}$
a
z

Density distributions in the slab phase

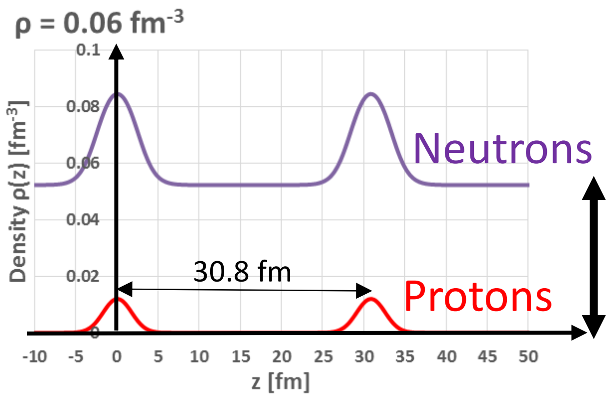

ρ = 0.06 fm^{-3}

Dripped Neutrons

Beta equilibrium

$$\mu_n = \mu_p + \mu_e$$
$$n \leftrightarrows p + e + \nu$$

$$Y_p = 0.02 - 0.04$$

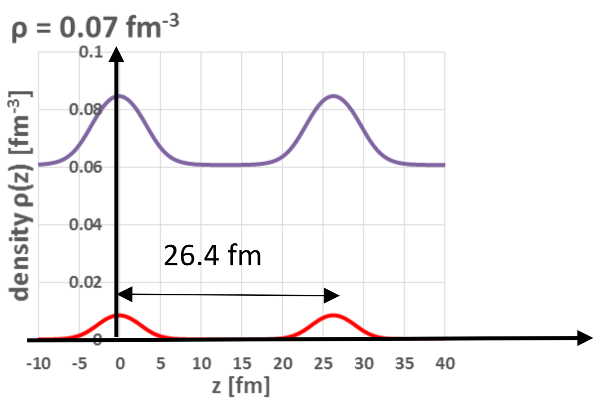

ρ = 0.07 fm^{-3}

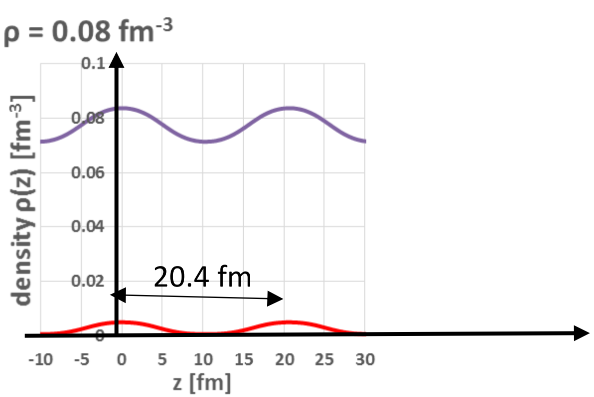

ρ = 0.08 fm^{-3}

Protons are also dripped near the transition to uniform matter

Neutron bands

$n_B = 0.07\ \mathrm{fm}^{-1}$

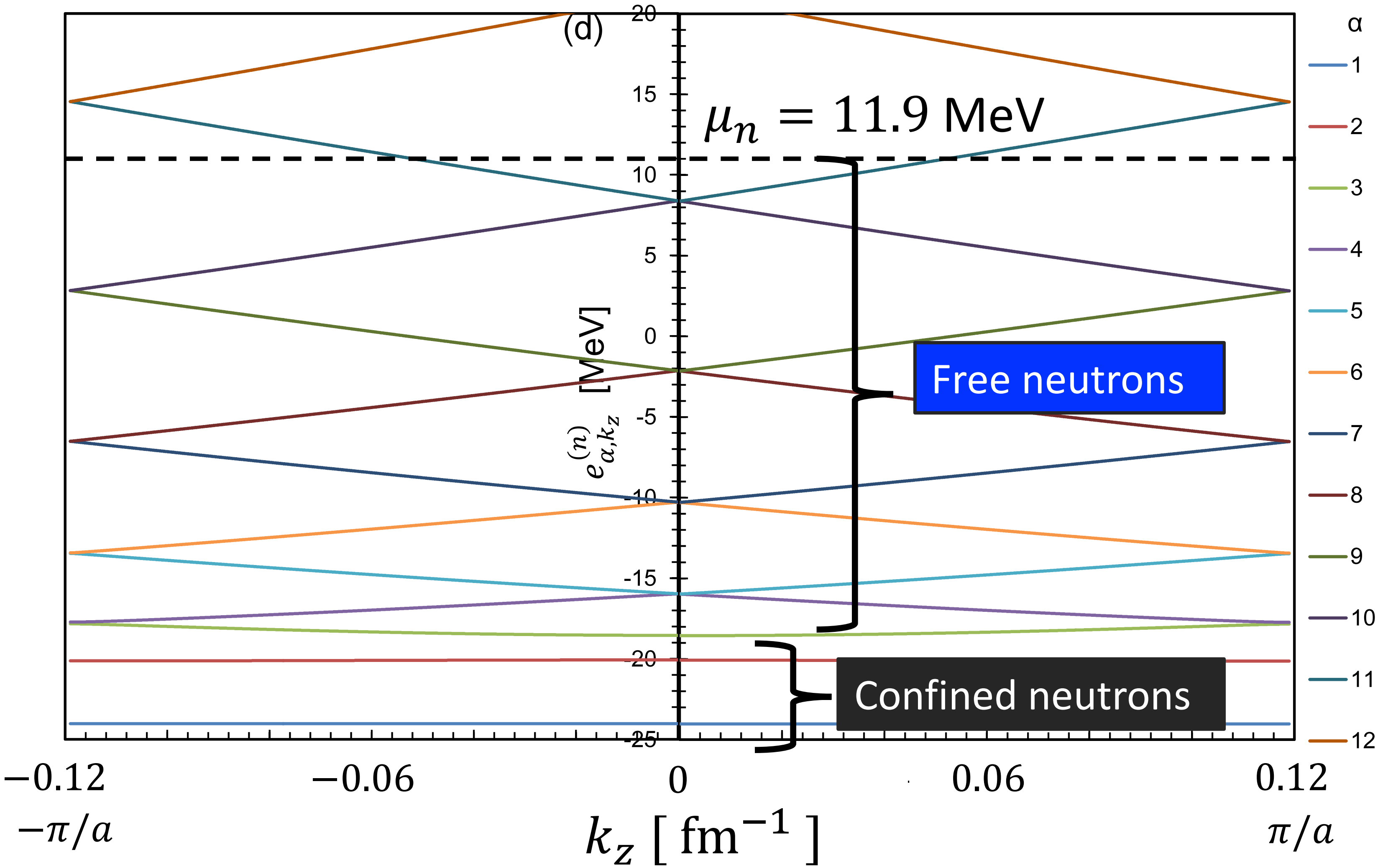

Effective mass

- Effective mass due to Bragg scattering

$$\boxed{\frac{m_n^*}{m_n} = \frac{n^f}{n^c}}$$

  - Conduction neutron density: $n^c = m_n K^{zz}$

$$\mathcal{K}^{zz} \equiv \frac{m_n}{\pi a N_k} \sum_{\alpha, k_z}^{\mathrm{occ}} \frac{d^2 e_{\alpha,k_z}^{(n)}}{dk_z^2} \left(\mu_n - e_{\alpha,k_z}^{(n)}\right),$$

  - Free neutron density: n^f

- Group velocity of neutrons

$$v_{\alpha,\boldsymbol{k}} = \nabla_{\boldsymbol{k}} \epsilon_{\alpha,\boldsymbol{k}}$$

  - Neutrons in "flat" bands are defined "Confined".

Effective mass

Kashiwaba, Nakatsukasa, Phys. Rev. C 100, 035804 (2019)

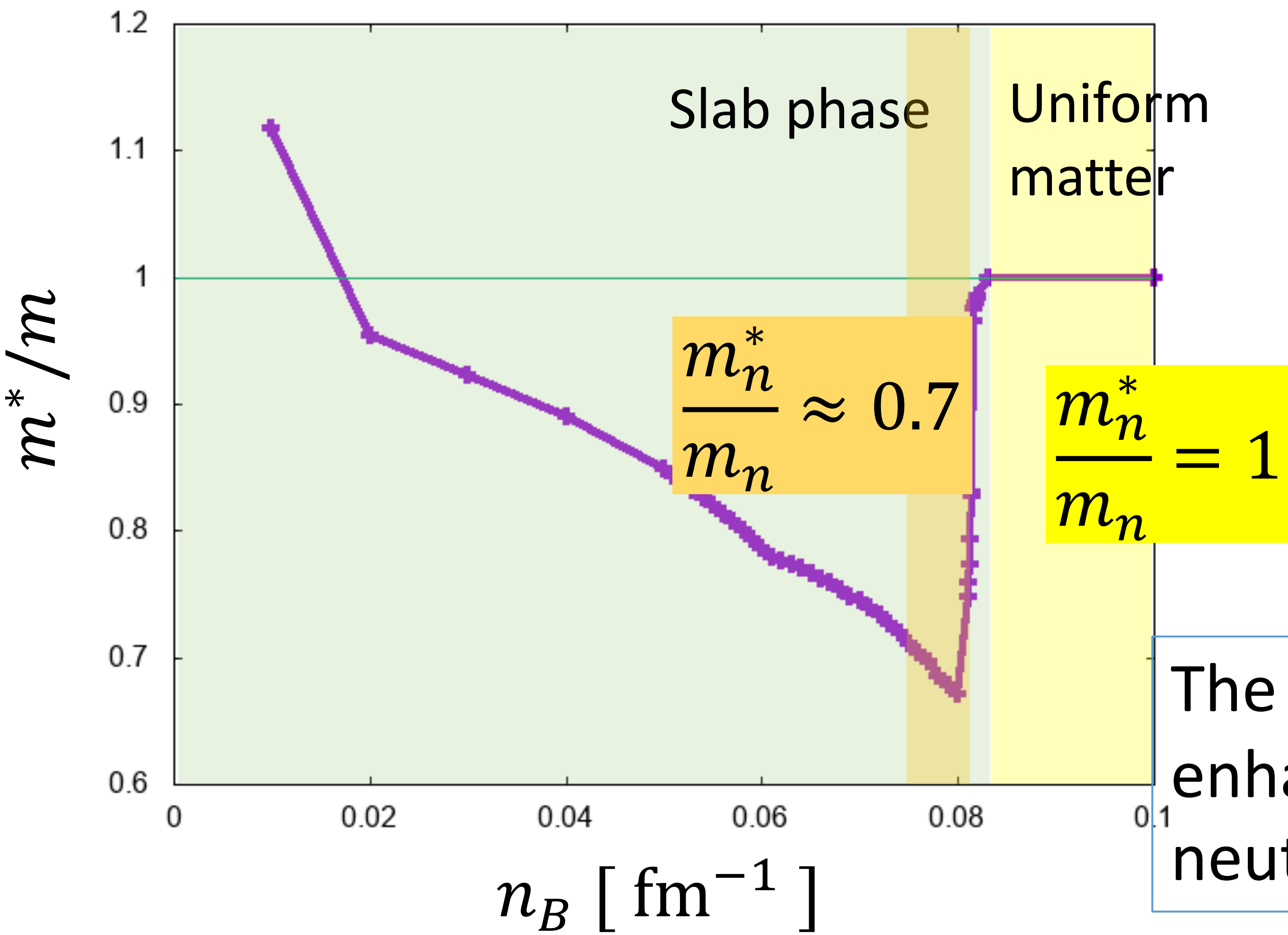

The Bragg scattering enhances the neutron mobility!

Anti-entrainment effect

Similar results with TDDFT calculation:
Sekizawa, Kobayashi, Matsuo, PRC 105, 045807 (2022)

Superfluidity (inclusion of pairing)

FOE method for HFB can be achieved by

$f_T(H)$ with H as HFB Hamiltonian

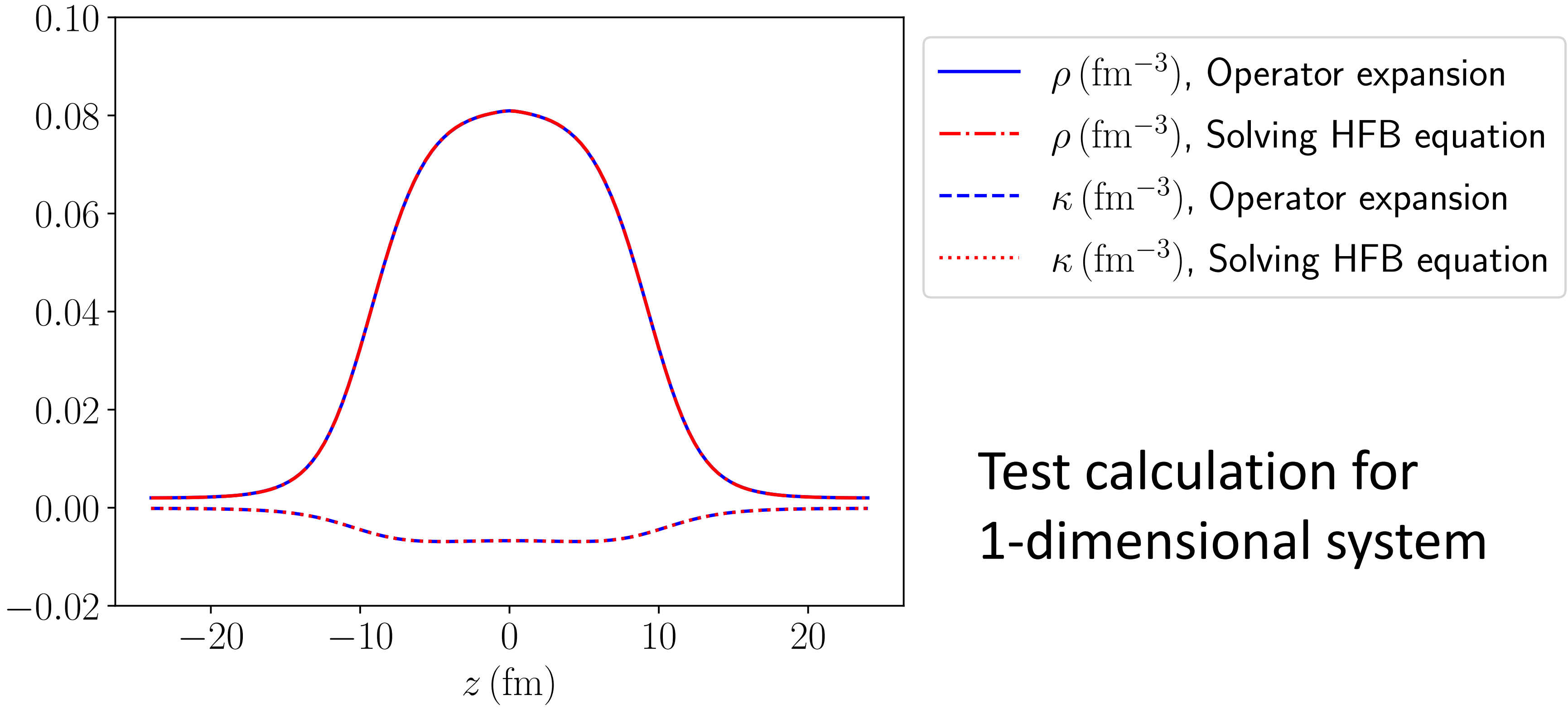

Test calculation for
1-dimensional system

Effect of superfluidity

- Superfluid neutrons may reduce the effective mass (Watanabe, Pethick, PRL 119, 062701, 2017)
- TDHFB cal. with accelerated protons [1D] (Yoshimura, Sekizawa, PRC 109, 065804 (2024)) $\Rightarrow$ Small effect
- Moving frame [1D] (Almirante, Urban, PRC 109, 045805 (2024)) $\Rightarrow$ Small effect

Superfluid current

- Introducing quasi-momentum $\boldsymbol{Q}$

$$\Delta(\boldsymbol{r}) \rightarrow \; \Delta(\boldsymbol{r}) e^{2i\boldsymbol{Q}\cdot\boldsymbol{r}}$$

- Supercurrent density: $\boldsymbol{j}(\boldsymbol{r})$

$$\frac{1}{V}\int_V \mathbf{j}(\mathbf{r}) d\mathbf{r} = \frac{n}{m^*}\mathbf{Q} = \frac{n_s}{m}\mathbf{Q}$$

n_s: Superfluid neutron density
n: Neutron density
m^*: Neutron effective mass

Superfluid neutron density

- Adopting the potential at $n_B = 0.07\ \mathrm{fm}^{-3}$

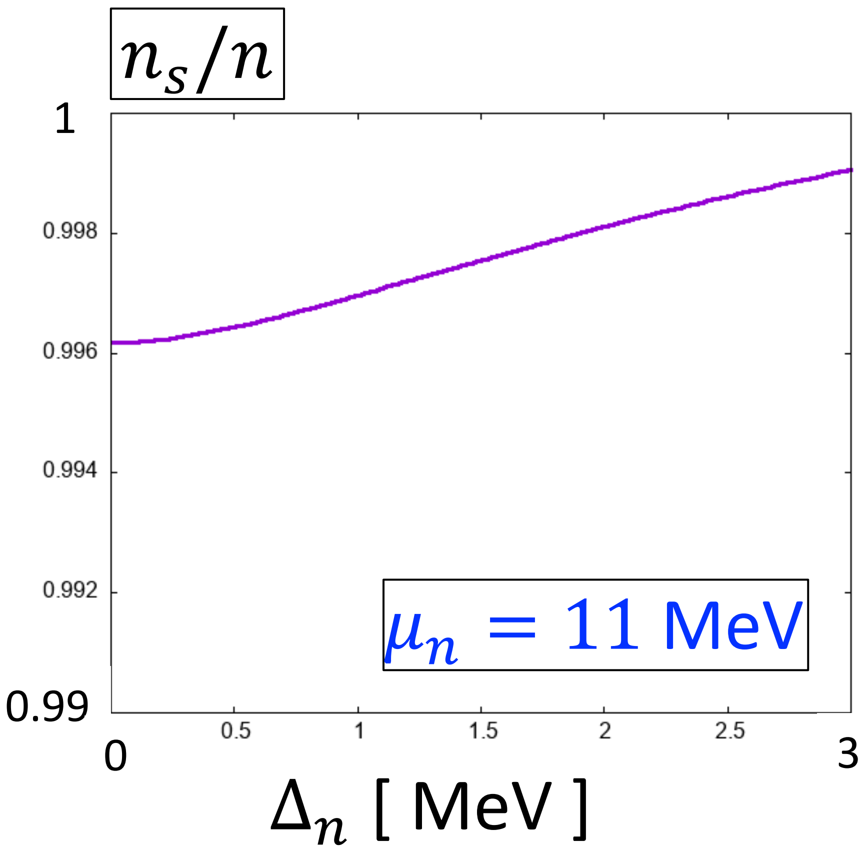

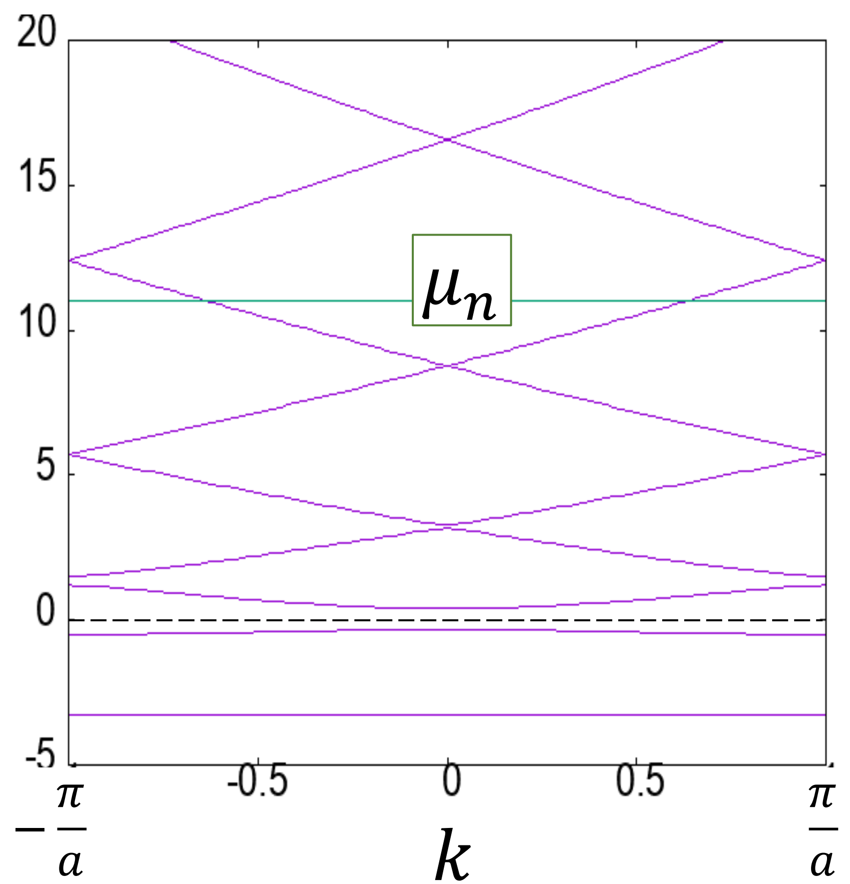

Superfluid neutron density

- Adopting the potential at $n_B = 0.07\ \mathrm{fm}^{-3}$

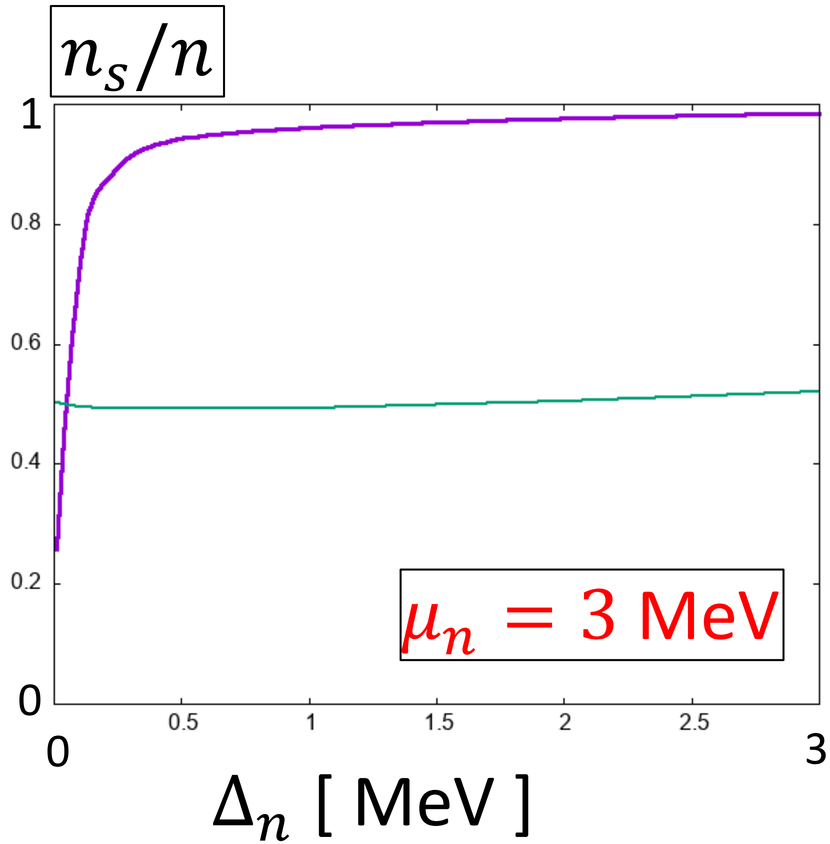

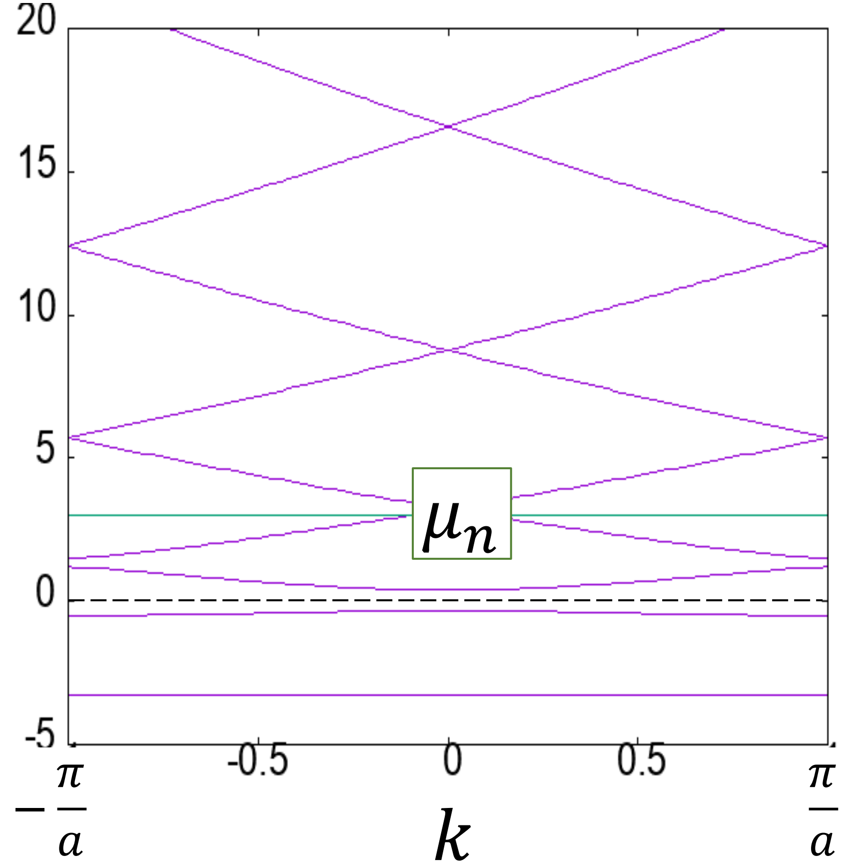

Effective mass for superfluid neutrons

N. Chamel, PRC 85, 035801 (2012)

$\bar{n}$ (fm^{-3})	Z	A	$n_n^{\rm f}/n_n$ (%)	$n_n^{\rm c}/n_n^{\rm f}$ (%)	$m_n^\star/m_n$
0.0003	50	200	20.0	82.6	1.21
0.001	50	460	68.6	27.3	3.66
0.005	50	1140	86.4	17.5	5.71
0.01	40	1215	88.9	15.5	6.45
0.02	40	1485	90.3	7.37	13.6
0.03	40	1590	91.4	7.33	13.6
0.04	40	1610	88.8	10.6	9.43
0.05	20	800	91.4	30.0	3.33
0.06	20	780	91.5	45.9	2.18
0.07	20	714	92.0	64.6	1.55
0.08	20	665	104	64.8	1.54

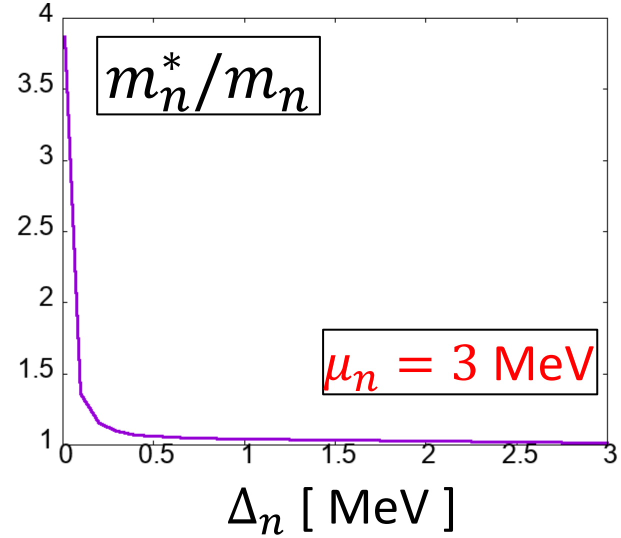

2~3.5 (?)

0.6~1

Superfluid effect: Reduction in effective mass (1/4 at low density)

Consistency with inner-crust origin of pulsar glitch phenomena

Full 3D calculation

- Various configurations (fcc, bcc, rod, slab, anti-rod, anti-fcc/bcc, etc.)
- Large 3D box
- Nuclear superfluidity
- Finite temperature

3D finite-temperature HFB calculation

- KSBdG (HFB) eq.

$$\begin{pmatrix} h-\mu & \Delta \\ -\Delta^* & -(h-\mu)^* \end{pmatrix} \begin{pmatrix} U_k \\ V_k \end{pmatrix} = E_k \begin{pmatrix} U_k \\ V_k \end{pmatrix}$$

- Densities

$$\rightarrow \rho = UfV^\dagger + V^*(1-f)V^T$$
$$\rightarrow \kappa = UfV^\dagger + V^*(1-f)U^T$$
$$f_{kk'} = \delta_{kk'}/\left(1+e^{\beta E_k}\right)$$

- Self-consistent iteration

- Diagonalization of the matrix
  - High computational cost
  - Low parallel efficiency

Green's function

- HFB Green's function

$$G(z;\xi,\xi') = \begin{pmatrix} G_{uu}(z;\xi,\xi') & G_{uv}(z;\xi,\xi') \\ G_{vu}(z;\xi,\xi') & G_{vv}(z;\xi,\xi') \end{pmatrix}$$

$$G_{\phi\psi}(z;\xi,\xi') = \sum_{k>0}\left[\frac{\phi(\xi)\psi^*(\xi')}{z-E_k} + \frac{\psi(\xi)\phi^*(\xi')}{z-E_k}\right]$$

- Identity

$$\boxed{(zI - H_{\mathrm{HFB}})G(z) = I}$$

Densities

Kashiwaba, Nakatsukasa, Phys. Rev. C 101, 045804 (2020)

$$R_T = \begin{pmatrix} \rho_T & \kappa_T \\ -\kappa_T^* & 1-\rho_T^* \end{pmatrix} = \frac{1}{2\pi i}\oint_C f_T(z) G(z) dz + T \sum_{|\omega_n|<h} G(i\omega_n)$$

$$f_T(z) = \left(1 + e^{\beta z}\right)^{-1}$$

Matsubara frequencies: $\omega_n = (2n+1)\pi T$

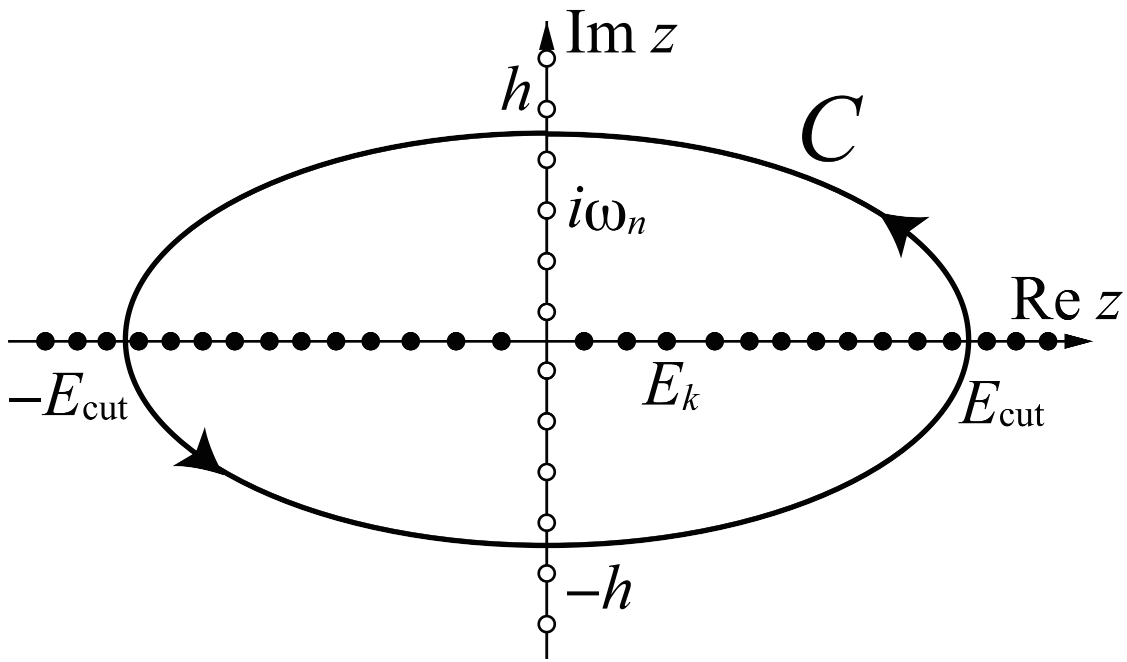

Pairing & shape transitions

Thermal pairing & shape transitions in ^{146}Ba

- On average, $C_V \propto T$
- Kinks in C_V at the pairing & quadrupole-shape phase transition points
- Disappearance of octupole shape has a minor effect on C_V

Kashiwaba, Nakatsukasa,
Phys. Rev. C 101, 045804 (2020)

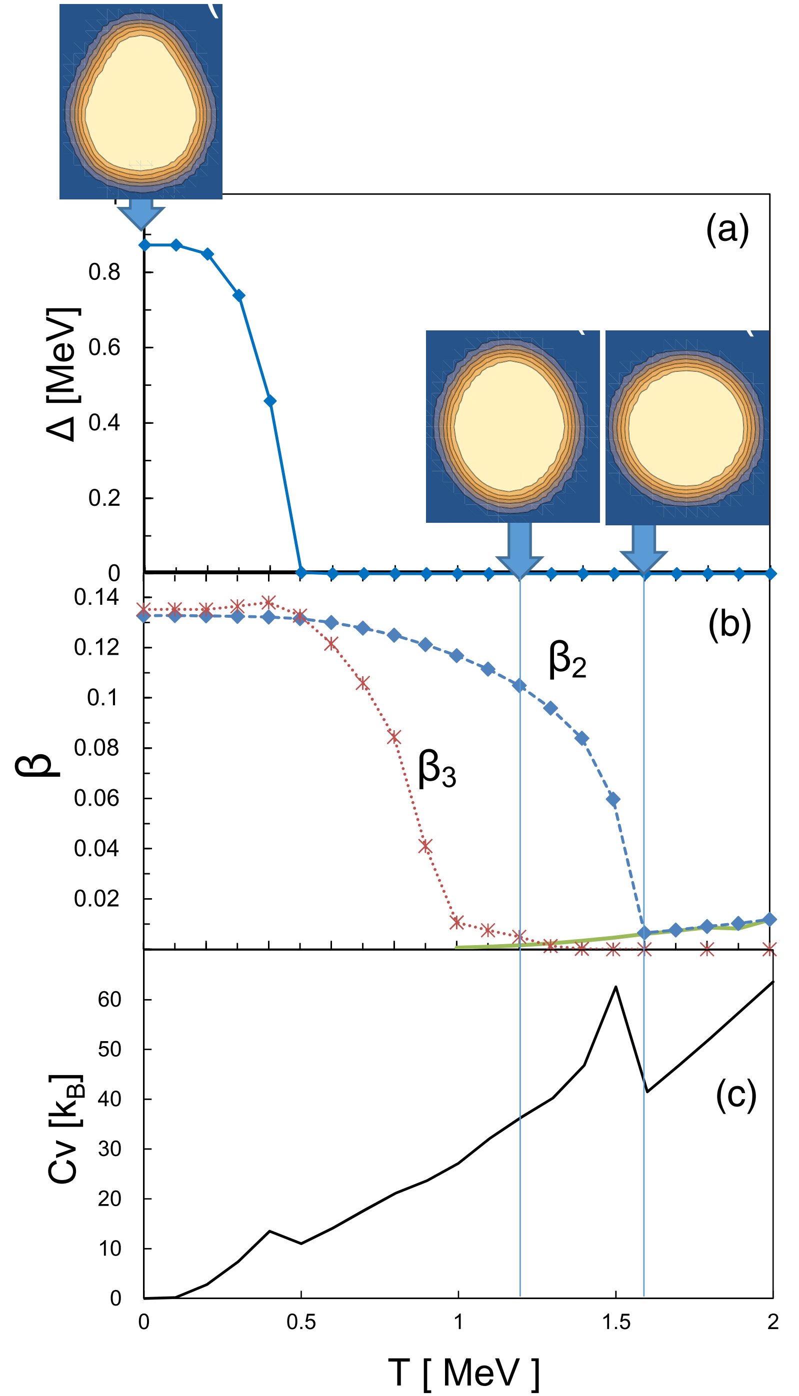

Benchmark calculation (fcc)

Kashiwaba, Nakatsukasa, Phys. Rev. C 101, 045804 (2020)

Beta equilibrium state with fcc in a cell of $(45\ \mathrm{fm})^3$

SLy4

Periodic boundary cond.

$T = 200$ keV

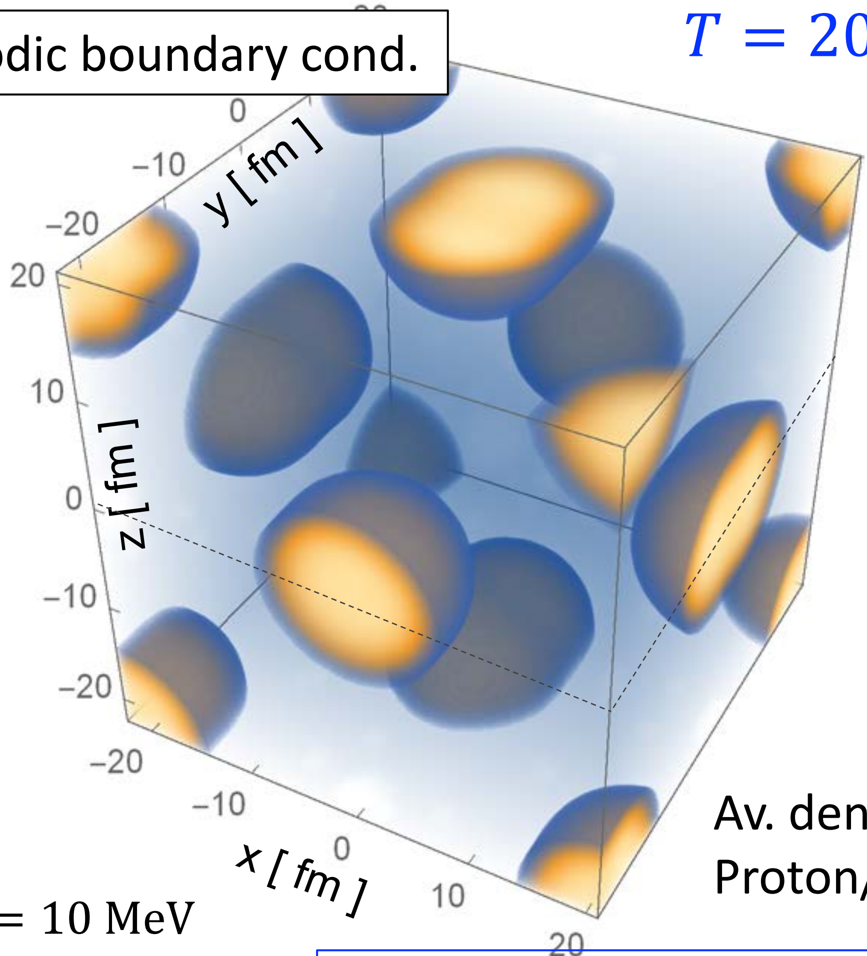

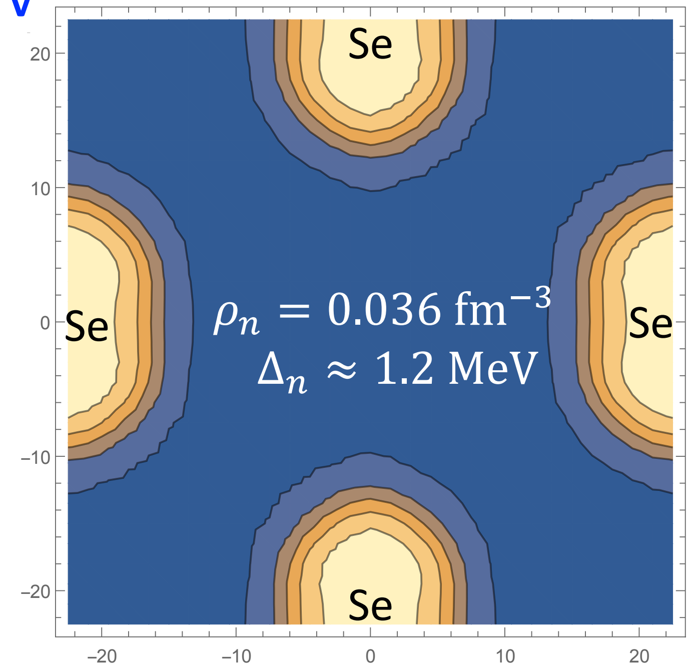

Av. density: $n_B = 0.045\ \mathrm{fm}^{-3}$

Proton/Neutron #: $Z = 136,\ N = 3936$

$\mu_n = 10$ MeV

Emergence of deformed Se nuclei “beyond drip line”

Higher density

Beta equilibrium state starting from fcc in a cell of $(45\ \mathrm{fm})^3$

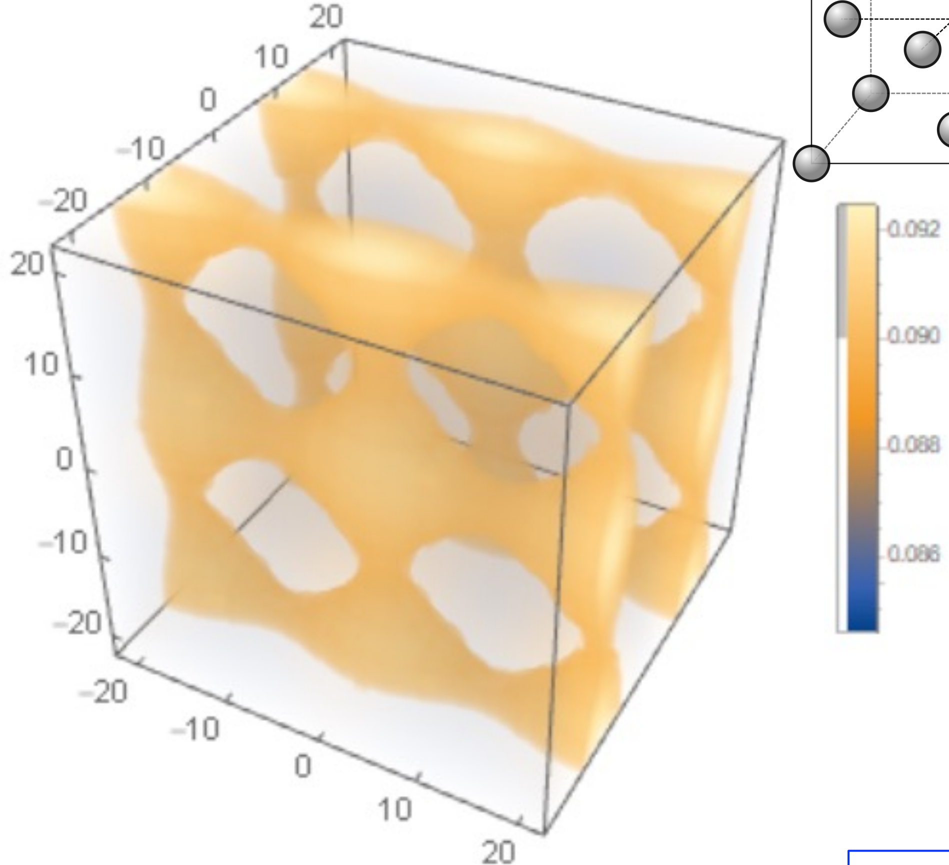

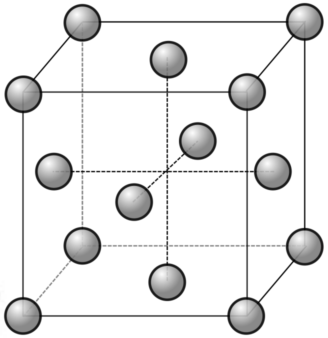

Neutron chemical potential:

$$\mu_n = 10\ \mathrm{MeV}$$
$$\downarrow$$
$$\mu_n = 14\ \mathrm{MeV}$$

Emergence of sliced swiss cheese

Summary

- Self-consistent band calculation for the slab phase of inner crust in neutron stars

  [Kashiwaba, TN, PRC 100, 035804 (2019)]

- Enhanced mobility by the entrainment effect

  $m^*/m \approx 0.7$ at $n_B = 0.07 - 0.08\ \mathrm{fm}^{-3}$

- Effect of superfluid neutrons

  Minor effect for slab phase: $n_B = 0.07 - 0.08\ \mathrm{fm}^{-3}$

  $m^*/m \approx 1/4$ at $n_B = 0.02 - 0.03\ \mathrm{fm}^{-3}$

  Possible revival of pulsar glitch model

- FT-HFB calculation in the 3D coordinate space representation
  - Green's function method [Kashiwaba, TN, PRC 101, 045804 (2020)]
  - Fermion operator expansion method [TN, PRC 107, 015802 (2023)]

Collaborators

- Chengpeng Yu (Postdoc at Univ. Tsukuba)
- Yu Kashiwaba (former PhD student)
- Mao Tsuchida (former Msc student)

University of Tsukuba
Center for Computational Sciences

筑波大学
University of Tsukuba

Multidisciplinary Cooperative Research & HPCI General Projects
筑波大学計算科学研究センター 学際共同利用 & HPCI一般利用課題

Oakforest-PACS System

Total peak performance			25 PFLOPS
Total number of compute nodes			8,208
Compute node	Product		Fujitsu PRIMERGY CX600 M1 (2U) + CX1640 M1 x 8 node
	Processor		Intel© Xeon Phi ™ 7250 (Code name: Knights Landing), 68 cores, 1.4 GHz
	Memory	High BW	16 GB, 490 GB/sec (MCDRAM, effective rate)
		Low BW	96 GB, 115.2 GB/sec (peak rate)
Interconnect	Product		Intel © Omni-Path Architecture
	Link speed		100 Gbps
	Topology		Fat-tree with (completely) full-bisection bandwidth
Parallel File System	Type		Lustre File System
	Total Capacity		26.2 PB
	Product		DataDirect Networks SFA14KE
	Aggregate BW		500 GB/sec
File Cache System	Type		Burst Buffer, Infinite Memory Engine (by DDN)
	Total capacity		940 TB (NVMe SSD, including parity data by erasure coding)
	Product		DataDirect Networks IME14K
	Aggregate BW		1,560 GB/sec
Power consumption			4.2 MW (including cooling)
# of racks			102

共同利用・共同研究拠点
「先端学際計算科学共同研究拠点」（文部科学省）
Advanced Interdisciplinary Computational Science Collaboration Initiative (the MEXT of Japan)

*Oakforest-PACSは、筑波大学計算科学研究センターと東京大学情報基盤センターが設置した最先端共同HPC基盤施設（JCAHPC）によって運用されています。
*Oakforest-PACS is operated by JCAHPC : Joint Center for Advanced High Performance Computing

JCAHPC